Check for updates

Second-Generation Transfer Mediates Efficient Propagation of ICE*Bs1* in Biofilms

Jean-Sébastien Bourassa,ᵃ Gabriel Jeannotte,ᵃ Sandrine Lebel-Beaucage,ᵃ Pascale B. Beauregardᵃ

ᵃDépartement de biologie, Faculté des sciences, Université de Sherbrooke, Sherbrooke, Québec, Canada

ABSTRACT   Horizontal gene transfer (HGT) by integrative and conjugative elements (ICEs) is an important mechanism in the spread of antibiotic resistance genes. However, little is known about the spatiotemporal dynamic of ICE propagation in bacterial biofilms, which are multicellular structures ubiquitous in natural and clinical environments. We report here that a high level of biofilm matrix production favors ICE*Bs1* acquisition. Also, using a fluorescently marked ICE*Bs1*, we observed that conjugation appears restricted to clusters of bacteria in a close neighborhood in which a high level of ICE*Bs1* transfer occurs. These conjugative clusters are heterogeneously distributed in the biofilm, forming close to the air-biofilm interface. Importantly, we established that transconjugant cells are the main contributors to ICE*Bs1* propagation in biofilms. Our findings provide a novel spatiotemporal understanding of ICEs propagation in biofilms, which should have an important role in our understanding of horizontal gene transfer in relevant settings.

IMPORTANCE   The transfer of mobile genetic elements between bacteria is the main cause of the spread of antibiotic resistance genes. While biofilms are the predominant bacterial lifestyle both in the environment and in clinical settings, their impact on the propagation of mobile genetic elements is still poorly understood. In this study, we examined the spatiotemporal propagation of the well-characterized ICE*Bs1*. Using the Gram-positive *Bacillus subtilis*, we observed that the main actors of ICE*Bs1* propagation in biofilms are the newly formed transconjugants that allow rapid transfer of ICE*Bs1* to new recipients. Our study provides a better understanding of the spatiotemporal dynamic of conjugative transfer in biofilms.

KEYWORDS   *Bacillus subtilis*, biofilm, ICE*Bs1*, integrative and conjugative elements, horizontal gene transfer

Horizontal gene transfer (HGT) is a fundamental phenomenon that drives the adaptation and evolution of bacteria in their environment (1). Conjugation is a preeminent HGT mechanism (2) that mediates the transfer of genetic material from a donor to a recipient cell upon direct cellular contact (3, 4). Since they encode complete mating machinery, conjugative plasmids and integrative and conjugative elements (ICEs) are genetic elements capable of self-transfer. They often carry accessory genes involved in metabolism, antibiotic resistance, and/or pathogenicity, which confer the cells bearing them a selective advantage (5–7). Consequently, they represent important actors in the emergence of multidrug resistance bacteria (8).

ICE*Bs1* is a 20.5-kb ICE present in multiple strains of *Bacillus subtilis*, a low G+C Gram-positive bacterium also able to form robust biofilms (9, 10). Since ICE*Bs1* gene function and regulation are very well understood, it constitutes an excellent model to study the propagation of ICE in Gram-positive bacteria (11). Activation of ICE*Bs1* can result from the activation of the SOS response following DNA damage in a RecA-dependent fashion (9, 11, 12). ICE*Bs1* activation is also mediated by RapI, a protein from the tetratricopeptide-repeat family encoded on ICE*Bs1* whose activity is inhibited by the small quorum-sensing peptide PhrI encoded downstream of *rapI* (9). Thus, the extracellular concentration of PhrI increases with

the number of ICE*Bs1*-containing cells in a population, ensuring that the transfer will not be activated if nearby cells already contain the element (9). Since PhrI is taken up prior to sensing, its propagation in space is limited, which leads to short-range communication (13).

Upon activation, ICE*Bs1* is excised from its integration site downstream of *trnS-leu2*, circularized, and then replicated by a rolling circle mechanism initiated at its origin of transfer (*oriT*) by the relaxase NicK (14). NicK is also involved in single-strand cleavage of the *oriT* to initiate the transfer via the type IV secretion system (T4SS) encoded by ICE*Bs1*, and the single-strand DNA is translocated to the recipient bacteria (15, 16). ICE*Bs1* is then recircularized before the complementary strand is synthesized (17–19). The newly completed ICE*Bs1* then integrates the chromosome via the *attB* site in the recipient genome. Importantly, transconjugants can also be immediately involved in another transfer to neighboring bacteria (3). In addition to the RapI-PhrI signaling, two other mechanisms limit ICE*Bs1* transfer to cells already bearing a copy of the element (20). The repressor ImmR mediates an immunity analogous to phage immunity (12), while YddJ, also encoded on ICE*Bs1*, mediates an exclusion mechanism by inhibiting the transfer from the ICE*Bs1* conjugation machinery (20).

Bacterial biofilms are microbial communities surrounded by a self-produced extracellular matrix (21, 22). Biofilms are ubiquitous in the environment and are involved in most chronic bacterial infections (23). Bacteria within these multicellular structures have an increased tolerance to antimicrobials, mainly due to the surrounding matrix, and this densely packed community provides rich intercellular interactions (22–25). Because of these characteristics, biofilms are favorable environments for HGT (4, 26, 27). Indeed, population-level analysis revealed that the transfer of conjugative plasmids was increased in various biofilms such as activated sludge communities, which are well-studied environmental biofilms (28–30). Examination of conjugative plasmid propagation in biofilms by using fluorescence microscopy and microfluidics revealed a low infiltration of the plasmids in an already established biofilm (29). In some cases, this poor efficacy was attributed to the low metabolic activity of recipient cells (31). However, other studies suggested that a low nutrient availability did not affect the transfer ability (26). While the capacity of conjugative plasmids to invade a biofilm appears limited, analysis of the conjugative plasmids RP4 and pKJK5 displayed efficient transfer in growing biofilms (28, 32). Of note, transconjugant cells were shown to have an important role in driving the transfer of RP4 in dual-species biofilm while having a minor impact in a complex activated sludge community (28). While these observations led to a better understanding of conjugation in biofilms, the spatiotemporal dynamics and factors impacting the conjugative transfer of ICEs in these multicellular communities have not yet been characterized (27).

We previously demonstrated that *B. subtilis* biofilm formation promotes the transfer of ICE*Bs1* and that the production of the biofilm matrix exopolysaccharide (EPS) and fibers (TasA) is required for this high efficiency (33). Here, we took advantage of the high propagation of ICE*Bs1* in *B. subtilis* biofilms to better understand the spatiotemporal parameters of conjugation in biofilms using fluorescence microscopy. We report that although biofilms are considered a favorable environment for conjugative transfer, ICE*Bs1* propagates in confined, relatively small areas that display a strong transfer level. We also observed that most conjugation events occur near the air-biofilm interface and that transconjugant bacteria are the key actors in the propagation of ICE*Bs1* in biofilms.

RESULTS

Bacteria-producing matrix components do not preferentially acquire ICE*Bs1*. In a previous study, we observed that the production of biofilm matrix by recipient cells, but not by donor cells, drives the strong conjugative transfer of ICE*Bs1* in biofilm. However, matrix expression is heterogeneous in a biofilm, and thus, we wanted to examine if ICE*Bs1* conjugative transfer would increase in a scenario where all recipient cells expressed matrix. We performed a conjugation assay with recipient cells deleted for *sinR*, the transcriptional repressor of the operons encoding exopolysaccharide
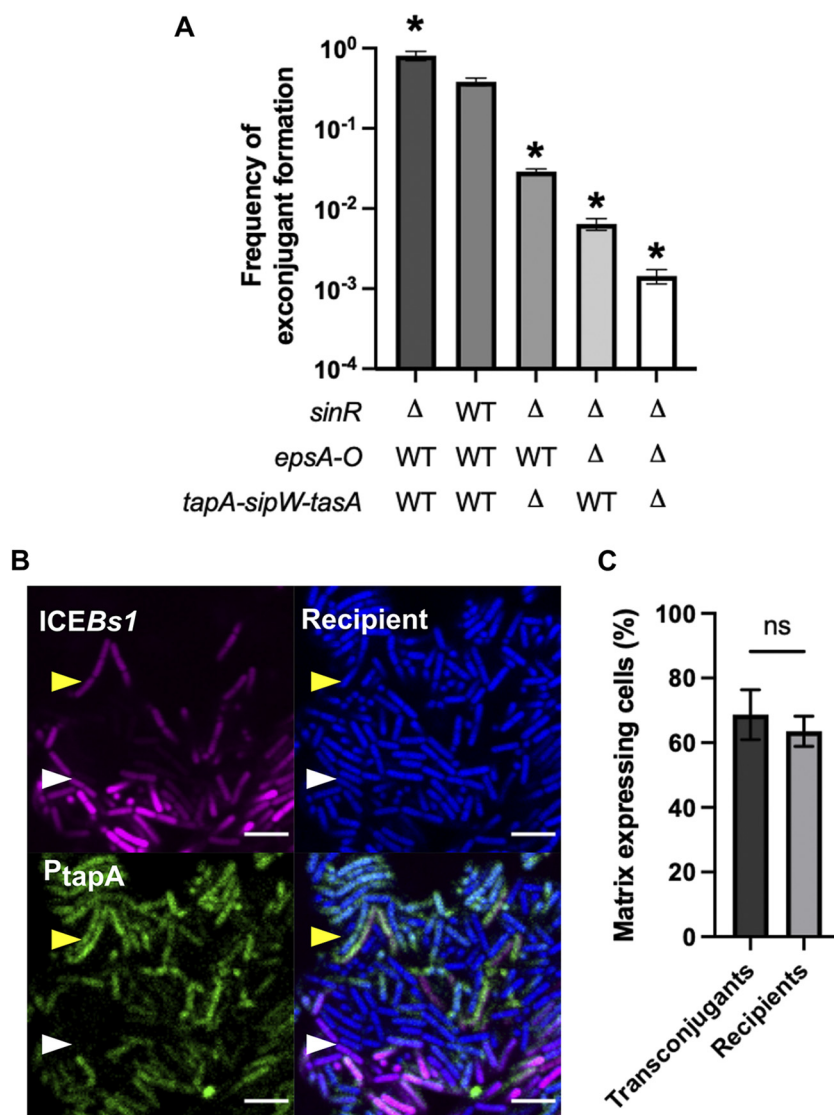
FIG 1 Influence of matrix production on ICE*Bs1* acquisition. (A) Mating between wild-type (WT) donor bacteria and recipient bacteria affected in their ability to produce biofilm matrix, incubated for 20 h on solid MSgg. The error bars represent the standard deviation of the mean (SD), and the results are representative of 3 biological replicates. Statistical analysis was done using a Brown-Forsythe and Welch's analysis of variance (ANOVA) followed by Dunnett's multiple-comparisons test. *, significant difference ($P \leq 0.05$) from the WT. (B) Mating between donor cells carrying ICE*Bs1-mkate2* (magenta) and recipient cells expressing *cfp* (blue) at a 1:5 donor-to-recipient ratio. Cells were incubated for 20 h on MSgg before imaging. Both donor and recipient also possess the P$_{tapA}$-*yfp* (green) biofilm reporter. The scale bar indicates a size of 5 μm. The white arrow shows a transconjugant that does not produce matrix, and the yellow arrow shows a transconjugant-producing matrix. The image is representative of more than 20 pictures of conjugative clusters from 3 independent biological replicates. (C) Proportion of transconjugant and recipient cells expressing matrix gene, as determined by enumeration of 9 conjugative clusters using microscopy images. Statistical analysis was done using paired *t* test; ns, $P > 0.05$. Error bars represent the SD, and the results are representative of 3 independent replicates.

biosynthesis (*epsA-O*), and protein fibers (*tapA-sipW-tasA*) of the matrix (34). Donor and recipient cells were mixed at a 1:5 ratio, and conjugation efficiency was examined after 20 h of incubation on a biofilm-inducing medium (MSgg). As seen in Fig. 1A, deletion of *sinR*, and thus overproduction of the extracellular matrix by all recipient cells, led to a significant increase (2-fold) in conjugative transfer. Deletion of one or both matrix operons in a Δ*sinR* background caused a decrease in transfer, suggesting that both matrix components are needed for a high transfer efficacy, and a high level of one component cannot palliate for the absence of the other.

To confirm the high ICE*Bs1* transfer to matrix-secreting recipient cells, we imaged conjugation and matrix production in parallel. The gene encoding the red fluorescent protein mKate2 was inserted in ICE*Bs1*, which allowed us to follow its propagation by microscopy. We noticed that ICE*Bs1-mKate2* had a slightly diminished transfer level compared to ICE*Bs1* bearing the *kan* resistance gene used previously, but it still displayed robust conjugation (see Fig. S1 in the supplemental material). To visualize recipient bacteria, we integrated at a genomic locus the gene encoding cyan fluorescent protein (CFP). Finally, the transcriptional reporter P$_{tapA}$-*yfp*, which transcribes the *yfp* gene when cells are producing at least one component of the biofilm matrix (24), was inserted in ICE*Bs1-mkate2* donors and *cfp* recipient cells. After a 20-h mating period, we inverted biofilms on a coverglass to directly image conjugation and determine the proportion of recipients and transconjugants expressing matrix genes (Fig. 1B). Since the biofilm matrix has a strong positive effect on transfer, we expected the proportion of transconjugant cells to express P$_{tapA}$-*yfp* more often than recipient cells. However, we did not observe a significant in the proportion of transconjugants cells expressing P$_{tapA}$-*yfp* from the proportion observed for all recipient cells (Fig. 1C). This discrepancy might be due to the fact that biofilm formation can be inhibited in transconjugants following the acquisition of ICE*Bs1* via expression of DevI, as previously reported by Jones et al., thus limiting the expression of the P$_{tapA}$-*yfp* reporter in transconjugant cells (35).

ICE*Bs1* transfer in biofilm occurs in clusters. Intriguingly, microscopy observation revealed that conjugation events in biofilms appeared to be concentrated in particular regions. To further examine this phenomenon, we used the ICE*Bs1-mKate2* reporter to image conjugation in cells incubated on biofilm and non-biofilm-inducing medium after 12 h, 16 h, and 20 h. In these assays, genes encoding CFP or green fluorescent protein (GFP) were integrated at a genomic locus of donor and recipient bacteria, respectively. After 12 h of incubation, we observed that ICE*Bs1* transfer was initiated in a few donor bacteria scattered through the biofilm and which showed strong mKate2 fluorescence; of note, most donor cells showed low fluorescent signal from mKate2 (Fig. 2A). This discrepancy between the fluorescence of various donor cells is likely due to the activation of ICE*Bs1* and its subsequent replication, which would increase the number of *mKate2* copies (36, 37). Four hours later, those initial donors had transferred ICE*Bs1* to neighboring cells, forming clusters of mKate2-positive (mKate2$^+$) cells (Fig. 2A). By 20 h, the clusters were enlarged, and almost all the bacteria included in the area were transconjugant cells, many of which also strongly expressed mKate2 (Fig. 2A). The propagation of ICE*Bs*1 was restricted to these active conjugative clusters (defined as containing at least 5 transconjugants) formed by donor cells surrounded by transconjugants.

We previously showed that matings performed on a nonbiofilm medium have 100-fold fewer conjugation events than mating on a biofilm-inducing medium (33). Similar to the biofilm medium, at 12 h on a nonbiofilm medium, we observed few donor cells with a high level of mKate2 fluorescence and very few transconjugants. At 16 h and 20 h, ICE*Bs1* was also disseminated to neighboring cells, but the conjugative clusters appeared significantly smaller than those formed on the biofilm medium (Fig. 2A). Further analysis confirmed that at 20 h in biofilm conditions, the conjugative clusters were composed of an average of 95 cells, while in nonbiofilm conditions, they contained approximately 20 cells (Fig. 2B). Our results show that ICE*Bs1* transfer in biofilm and nonbiofilm conditions was confined into clusters, but these were significantly larger in biofilm conditions.

ICE*Bs1* transfer in biofilm is heterogeneous. Imaging of biofilm inverted on a microscope coverslip does not recapitulate the complexity of the biofilm structure, which is a very heterogeneous environment. Thus, the presence of conjugative clusters in a fully formed colony biofilm was examined using transversal imaging. Matings were performed by dropping a mix of donor and recipient cells, bearing the same fluorescent reporters as described in Fig. 2, at a 1:5 ratio on a solid biofilm-inducing medium. Biofilms were fixed and included in optimal cutting temperature (OCT) compound after
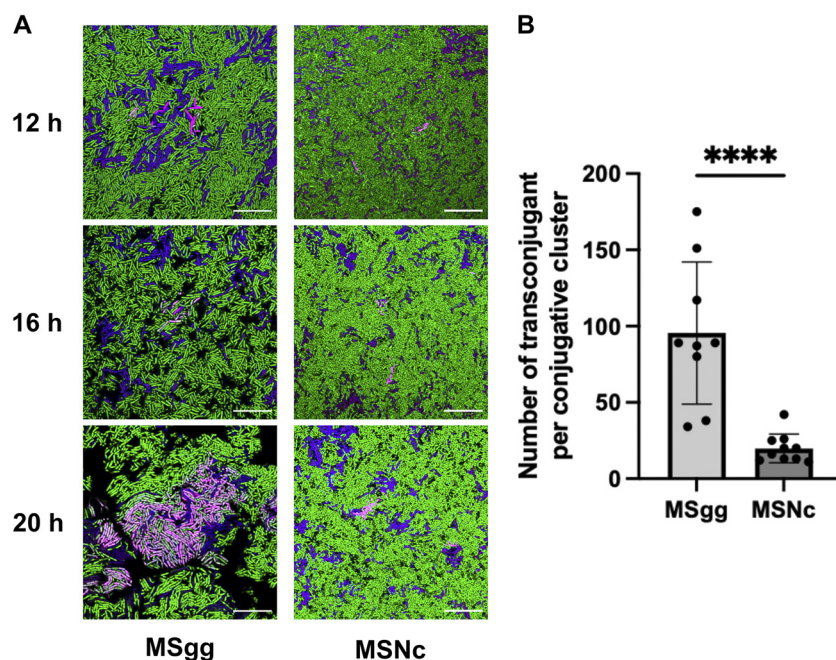
FIG 2 ICE*Bs1* transfer occurs in clusters. (A) Donor strains expressing *cfp* from a genomic locus and bearing ICE*Bs1-mkate2* were mated at a 1:5 donor-to-recipient ratio with a recipient strain expressing *gfp* and visualized by fluorescence microscopy after 12 h, 16 h, and 20 h at 30°C on biofilm (MSgg) and nonbiofilm (MSNc) media. Donor cells appear blue to purple if the expression of mKate2 is low and magenta if there is a strong mKate2 fluorescence; recipients are shown as green, and transconjugants appear either light pink if having a strong mKate2 fluorescence or gray for a weak mKate2 fluorescence. Scale bars indicate a size of 10 μm. Images are representative of at least 9 fields of view from 3 independent experiments. (B) Transconjugants composing the different conjugative clusters, as imaged in panel A, were enumerated on biofilm (MSgg) and nonbiofilm (MSNc) media. At least 9 fields of view from 3 independent experiments were used, and each dot represents a cluster of at least 5 transconjugant cells. Statistical analysis was done using a *t* test; ****, $P < 0.001$. Error bars represent the standard deviation (SD).

12 h, 16 h, 20 h, 24 h, and 28 h of incubation, and thin sections of the biofilms were prepared using a cryomicrotome to obtain slices containing a view of the entire depth of the biofilm. Slices were then mounted between a slide and the coverslip with an aqueous montage solution for imaging by confocal microscopy.

After 12 h of incubation, donor bacteria with strong mKate2 fluorescence were disseminated through the biofilm, but there were few transconjugants, similar to what was observed in inverted biofilms (Fig. 3A). After 16 h of incubation, small independent clusters of mKate2$^+$ (magenta) cells composed of donors and transconjugants were visible (Fig. 3A and B). Longer biofilm incubation times led to larger clusters composed of transconjugant cells, suggesting a strong multiplication of transconjugants and/or a sustained transfer of ICE*Bs1-mkate2* (Fig. 3A and B). Of note, most of these clusters appeared to have a vertical expansion and to be heterogeneously distributed in the biofilm. Positional analysis was performed on the clusters by measuring the distance between the top of the cluster and the air interface (Fig. 3C, light blue) and between the bottom of the cluster and the medium interface (purple). The results clearly demonstrate that most clusters were found close to or directly at the air-biofilm interface of the biofilm, while the bottoms of the cluster were more randomly distributed, respectively, to the medium interface (Fig. 3C).

Second-generation transfer mediates efficient ICE*Bs1* propagation inside the biofilm. Using three-dimensional (3D) imaging of the conjugative cluster on inverted biofilm, we noticed that many transconjugant cells were not adjacent to donor cells (Video S1). This observation suggests that the transfer of ICE*Bs1* mediated by transconjugants could play an important role in ICE*Bs1* propagation in biofilms. To examine the importance of this second-generation transfer, we designed a conjugation assay in which only the donor cells, but not the transconjugants, could transfer ICE*Bs1*. We first
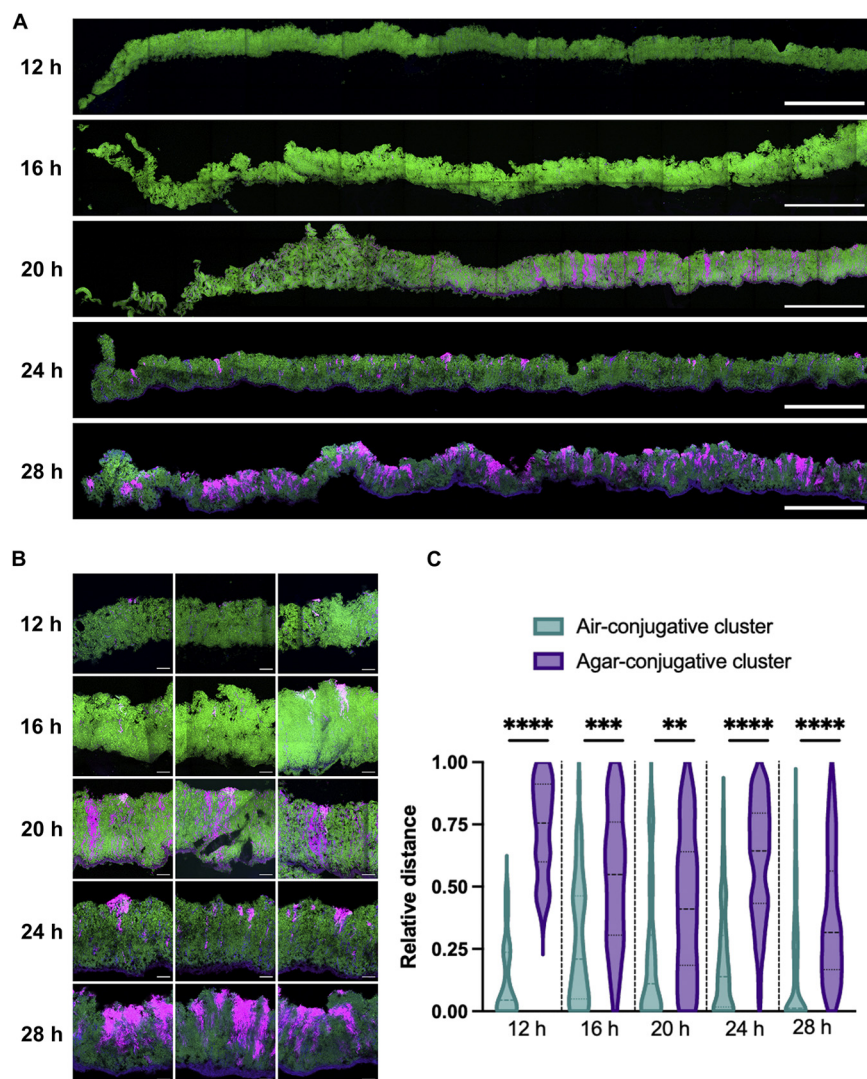
FIG 3 Spatiotemporal analysis of ICE*Bs1* propagation within a biofilm. Vertical thin section of biofilm composed of donor cells expressing ICE*Bs1-mkate2* with recipient cells expressing a *gfp* gene at a 1:5 donor-to-recipient ratio. At the indicated time, biofilms were fixed prior to cryosectioning. (A) Wide view of the thin section representing approximately one-third of the biofilm diameter, starting from the edge (left) toward center (right). (B) Closeup of the conjugative clusters. Donors appear purple, recipients are shown in green, and transconjugants are in light pink to gray color; for each image, the air-biofilm interface is at the top, and the biofilm-agar interface is at the bottom. The scale bars indicate a size of 250 μm (A) and 20 μm (B). (C) Relative distance of the conjugative cluster from the air-biofilm (light green) or agar-biofilm (purple) interface. Relative distance is reported as the distance separating the conjugative cluster to the interface relative to the depth of the biofilm at the cluster's location. The darker dotted lines represent the median, and lighter dotted lines represent the 25th and 75th percentiles. Results are a compilation of at least 19 conjugative clusters from at least 3 independent biofilms. Statistical analysis was done using a *t* test and shows that the bacterial cluster is closer to the air-biofilm interface than the agar-biofilm interface. (**, $P < 0.01$; ***, $P < 0.001$; ****, $P < 0.0001$).

performed an in-frame markerless deletion of *conG*, a gene present on ICE*Bs1* which encodes an essential protein of its conjugative machinery (16). The *conG* complementation was constructed in *trans* under the control of the inducible promoter P$_{hyperspank}$. As previously reported, deletion of *conG* completely abrogated ICE*Bs1* transfer, but the presence of *conG* in *trans* in both the donor and recipient cells restored conjugation to wild-type levels (Fig. 4A). Importantly, if the complementation was only present in the donor cells, ICE*Bs1*Δ*conG* was able to transfer from donor cells to recipient cells, but the newly formed transconjugants were unable to further propagate ICE*Bs1*Δ*conG*. Using this approach, we observed a significant decrease in the conjugation efficiency
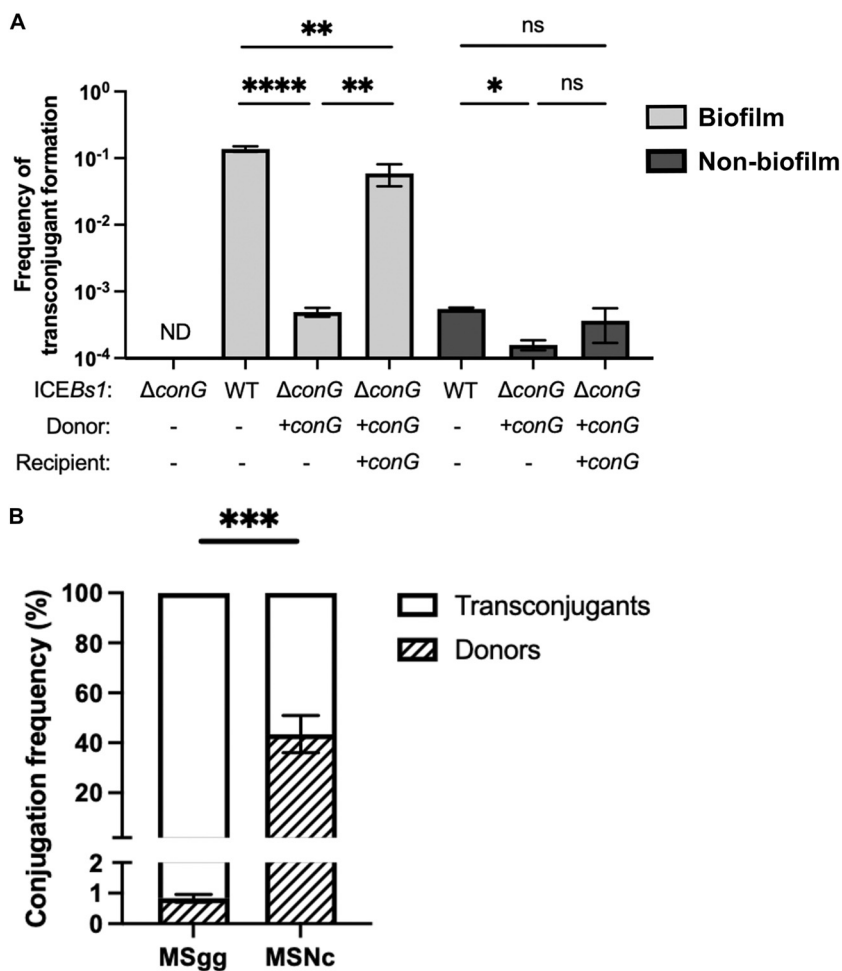
FIG 4 Transconjugants play a major role in ICE*Bs1* propagation. (A) Donor cells with an in-frame deletion of *conG* in ICEBs1 (Δ*conG*) were complemented in *trans* by expressing *conG* under the control of an IPTG-inducible promoter inserted at the *amyE* locus (+*conG*). Cells were mixed at a 1:5 donor-to-recipient ratio on a biofilm (MSgg, light gray) or a nonbiofilm (MSNc, dark gray) medium with 50 μM IPTG induction. Statistical analysis was performed using one-way ANOVA test followed by Tukey's multiple-comparison test; (*, $P < 0.05$; **, $P < 0.01$; ****, $P < 0.0001$; ND; nondetectable). (B) The proportion of conjugation attributed to donor and transconjugant cells was calculated by determining the relative contribution of donor conjugation (+*conG* in donor cells only) to total conjugation (+*conG* in donor and recipient cells). Statistical analysis was done using an unpaired *t* test; ***, $P < 0.001$. Results showed are representative of at least three independent replicates.

in biofilm and nonbiofilm conditions when *conG* was complemented only in donor cells compared to when it was complemented in both donor and recipient cells (Fig. 4A). This result confirmed that transconjugant bacteria propagate ICE*Bs1* after its acquisition. Importantly, transfer by transconjugant cells represented about 99% of ICE*Bs1* transfer in biofilm conditions, while it represented only 43% of the transfer in nonbiofilm conditions (Fig. 4B). These results indicate that ICE*Bs1* propagation in biofilm is mediated by a rapid spread via transconjugant cells.

It was previously reported that ICE*Bs1* can be efficiently transmitted via transconjugants by spreading rapidly through bacterial chain cells (3). Since *B. subtilis* can adopt this morphology in biofilm (38), we investigated if our observation of the importance of second-generation transfer could be explained by propagation in cell chains. Thus, we used single and combinatorial deletion mutants of genes (*lytABC*, *lytD*, *lytE*, and *lytF*) which encode autolysins responsible for the peptidoglycan cleavage following cell division, allowing the cells to separate (39, 40). While these deletion mutants forced the formation of cell chains (Fig. S2A), they did not display an increase in ICE*Bs1* transfer in nonbiofilm conditions (Fig. 5A). Similarly, overexpression of the autolysin
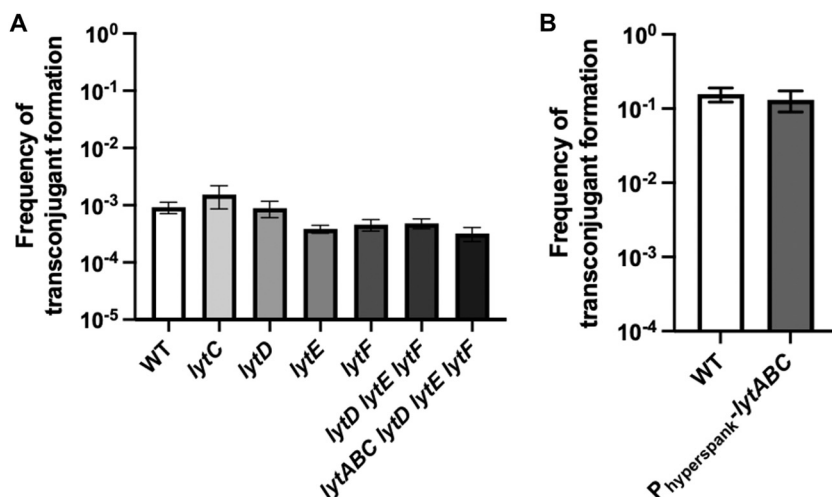
FIG 5 Cell chains are not involved in the propagation of ICE*Bs1* in a biofilm. (A) WT donor cells were mated with recipient cells lacking different autolysins and incubated on a nonbiofilm (MSNc) medium. (B) WT donor cells were mated with recipient cells overexpressing *lytABC* under the control of an IPTG-inducible promoter and incubated on a biofilm-inducing (MSgg) medium with 50 μM IPTG. For panels A and B, cells were mixed at a 1:5 donor-to-recipient ratio and incubated for 20 h at 30°C. Statistical analysis was performed using an ANOVA for panel A and *t* tests for panel B; (ns, $P > 0.05$) and showed no difference. The results shown are representative of at least 3 independent experiments, and error bars represent the standard deviation (SD).

locus *lytABC* in biofilm formation conditions did not impair the ability of ICE*Bs1* to transfer in biofilms (Fig. 5B) while reducing the presence of cell chains in biofilm conditions (Fig. S2B). From these results, we conclude that ICE*Bs1* transfer by transconjugant is key for its efficient propagation in biofilms but that this effect is not mediated by cell chains.

DISCUSSION

The molecular mechanisms underlying conjugation are well understood for many mobile genetic elements, but little is known about the spatiotemporal parameters of their propagation in more natural contexts (27). Here, we used the well-characterized ICE*Bs1* and its host, *B. subtilis*, to demonstrate that although propagation of ICE*Bs1* in biofilm is extremely efficient, its transfer is confined to clusters of cells where ICE*Bs1* replicates and rapidly spreads through transconjugant bacteria.

We recapitulated our previous observations that the production of matrix by recipient cells plays an important role in the propagation of ICE*Bs1* in biofilm. Using a deletion of *sinR* to force production of biofilm matrix, we uncoupled general phenotypic differentiation from *epsA-O* and *tapA-sipW-tasA* expression, further confirming the importance of the matrix components (Fig. 1A). However, microscopy observations revealed that transconjugants did not systematically express matrix genes, which might reflect the activity of the ICE*Bs1*-encoded *devI*. DevI was recently shown to inhibit expression of genes related to sporulation and biofilm formation, including *epsB* and *tasA*. Following ICE*Bs1* acquisition and *devI* expression in transconjugant cells, DevI then inhibits biofilm formation and sporulation, thus providing a fitness advantage, allowing cells bearing ICE*Bs1* to grow more (35). Our current hypothesis is that matrix would be required only at the beginning of transfer to stabilize the contact between donor and recipient cells.

We observed that ICE*Bs1* forms conjugative clusters, which are mostly located close to the air-biofilm interface, showing a clear heterogeneity in vertical distribution (Fig. 3C). Many of these conjugative clusters also display an uneven appearance with a preference for vertical expansion, which could suggest a polar growth of the transconjugant cells, a polar transfer, or both (Fig. 3B). Similarly, propagation of the TOL plasmid pWWO in an already formed biofilm also appeared to be confined to the few upper

layers of cells at the liquid medium interface of the biofilm (29). A lack of nutrients and oxygen inside the biofilm was proposed as an explanation for the confine transfer of pWWO at the liquid medium interface since the conjugative transfer requires a high energy cost (22). In our mating assay on solid biofilm-inducing medium, nutrient availability does not appear to influence ICE*Bs1* conjugative transfer since the cells present in the upper part of a colony biofilm have access to the least nutrients. Indeed, sporulation occurs rapidly in this specific biofilm layer (24). However, the air-biofilm interface was also shown to be the site of early TasA expression and faster accumulation of the biofilm matrix (24), which could explain the preferential localization of clusters close to this interface prior to occurrence deeper in the biofilm.

We observed that, initially, in biofilm, only a small number of bacteria produce a bright mKate2 fluorescent signal resulting from ICE*Bs1* excision and its replication in plasmid form (Fig. 2). This low number is in agreement with our previous observation that ICE*Bs1* is excised in less than 0.1% of the donors in both biofilm and nonbiofilm conditions (33). These initial events might be driven by the local density of donor and recipient cells since a high density of donor cells will lead to a repressing extracellular concentration of PhrI (9, 13). A similar observation was reported for the conjugative plasmid RP4 whose propagation in a growing biofilm also appears to arise from distinct areas prior to the expansion through most of the biofilm (28). Since transconjugant clusters can expand to almost a hundred cells, repression by PhrI is unlikely to have an effect on second-generation transfer. We hypothesize that this phenomenon could be explained by the kinetic repression by PhrI, which needs to be synthesized, exported, and then imported back to inhibit RapI, a process that might be slower than the conjugative transfer of an already active ICE*Bs1* present in transconjugants.

ICE*Bs1* propagation mediated by transconjugant cells was previously shown, but its importance for overall conjugative transfer was not evaluated (3). Our approach allowed us to precisely determine that the transfer initiated by transconjugant cells represents more than 99% of the total conjugative events observed in a biofilm (Fig. 4B). Because of the significant fitness advantage provided by ICE*Bs1* in biofilm, one could hypothesize that transconjugant cells would be abundant in the biofilm despite absence of second-generation transfer (35). However, our results confirm that second-generation transfer, and not the inherent growth advantages, explains the large number of transconjugant cells in biofilm. Additionally, even if ICE*Bs1* can rapidly spread through bacterial cell chains (3), this ability does not appear to contribute significantly to conjugation in biofilms (Fig. 5). Of note, a complementation of ICE*Bs1*-encoded ConG in donor cells was previously shown to restore completely the conjugation efficiency in filter mating (16), suggesting that the importance of second-generation transfer under nonbiofilm conditions might be condition dependent.

The high transfer efficiency by transconjugants might be explained by the initial absence of the negative regulator ImmR, upon transfer to a new cell (41). Following translocation, ICE*Bs1*, in its plasmid form, will be able to maintain its activated state, replicating and transferring efficiently, as proposed in another study (3). A high replication before the conjugative transfer was also observed for ICE*clc*, an ICE present in *Pseudomonas putida* that induces a transfer-competent (tc) differentiation in donor bacteria after activation of ICE*clc* genes (42). Activation of these genes led to a transient replication step prior to the conjugative transfer (43). Thus, bacteria in which ICE*clc* replicates are most likely to propagate the element. While ICE*Bs1* replication in the donor bacteria was shown to be unnecessary for the conjugative transfer of this element (44), a high copy number of ICE*Bs1* in transconjugants could favor the high secondary transfer while also supporting integration in the genome (19, 44). Our current model is that the strong ICE*Bs1* transfer in biofilm results from the combination of high ICE*Bs1* activity in newly formed transconjugant cells with the stabilizing effect of the extracellular matrix on cell-to-cell contacts between transconjugants and recipient cells.

While ICE*Bs1* propagation is driven by transconjugants, it is not the case for most conjugative elements. Previous reports showed complete recovery of the conjugative

levels of multiple elements upon deletion of a protein from their T4SS machinery and complementation only within the donor cells (45–47). These elements are members of multiple incompatibility groups present in both Gram-positive and Gram-negative bacteria, which indicates that a high level of second-generation transfer might be key for a certain subset of conjugative elements. However, these complementation assays were done in nonbiofilm conditions; since our study demonstrates that the epidemic transfer is important, particularly in biofilm, more investigation might reveal if it is a biofilm-specific feature of conjugation or not.

Our study provides new insights into the spatiotemporal dynamic of conjugative element propagation in biofilms. Since biofilms are ubiquitous in clinical environments where multiresistant bacteria can emerge, a better understanding of ICE propagation under these conditions is required to develop efficient strategies to prevent or decrease horizontal gene transfer. Further studies on the epidemic transfer of ICEs to better understand their real impact in natural environments are warranted.

MATERIALS AND METHODS

Strains and media. The strains used in this study were derived from the ancestor strain NCIB3610 (see Table S1 in the supplemental material). The bacterial growth media used is Luria-Bertani medium (LB; 1% [wt/vol] tryptone, 0.5% [wt/vol] yeast extract, and 0.5% [wt/vol] NaCl), and the different media used for mating assays were MSNc (5 mM potassium phosphate buffer, pH 7, 0.1 M morpholinepropane-sulfonic acid [MOPS], pH 7, 2 mM $MgCl_2$, 50 μM $MnCl_2$, 1 μM $ZnCl_2$, 2 μM thiamine, 700 μM $CaCl_2$, 0.2% [wt/vol] NH_4Cl, and 0.5% [wt/vol] cellobiose) (48) and MSgg (5 mM potassium phosphate buffer, pH 7, 0.1 M MOPS, pH 7, 0.025 mM $FeCl_3$, 2 mM $MgCl_2$, 50 μM $MnCl_2$, 1 μM $ZnCl_2$, 2 μM thiamine, 700 μM $CaCl_2$, 0.5% [vol/vol] glycerol, and 0.5% [wt/vol] glutamate) (38) solidified with 1.5% (wt/vol) agar. When needed, the following antibiotics were added to the media: MLS (1 μg mL^{-1} erythromycin and 25 μg mL^{-1} lincomycin), spectinomycin (100 μg mL^{-1}), chloramphenicol (5 μg mL^{-1}), and kanamycin (10 μg mL^{-1}).

Strain and plasmid construction. Most *B. subtilis* strains were made by transferring genetic constructions into NCIB3610 using SPP1-mediated generalized transduction (49). JMA384 (ICE*Bs1::kan*) was a gift from Alan D. Grossman's lab (Massachusetts Institute of Technology, MA); BJM396 (*lytC*), BJM402 (*lytD*), BJM76 (*lytE*), and BJM104 (*lytF*) were gifts from David Rudner's lab (Harvard Medical School, MA). pminiMAD2 (50) was a gift from Richard Losick's lab (Harvard, MA). The *Escherichia coli* strain used for routine cloning was NEB 5α (New England Biolabs). The plasmids used in this article are listed in supplemental material (Table S2). *tapA-sinR* deletion was created by long-fragment homology PCR. The flanking regions were amplified using P746-P747 and P748-P749, respectively, and the *erm* was amplified from pDG646. Plasmid constructions were done using pDR111 as the backbone plasmid unless indicated. *mkate2* was cloned into ICE*Bs1* by subsequent cloning of upstream and downstream regions of *yddM-yddN*. The upstream fragment was amplified with P342 and P343 primers and inserted at the BamHI restriction site downstream of *lacI*. The downstream fragment was amplified with primers P344 and P496 and was inserted while replacing the *amyE down* homology fragment with the AsisI and SacI restriction enzymes. P$_{hyperspank}$-*mkate2* was amplified from PB396 (*amyE::P$_{hyperspank}$-mkate2*) with primers P507 and P508 and inserted between the EcoRI and SphI restriction sites of pDR111. To complement the *conG* deletion, *conG* was amplified with primers P719 and P673 and inserted between the SalI and SphI restriction sites downstream of the P$_{hyperspank}$-inducible promoter on pDR111. P$_{hyperspank}$-*cfp* was obtained by amplifying *cfp* from pKM008 with primers P615 and P616 and cloned between HindIII and SphI restriction sites. HindIII is present in the amplification and not on primer P615. Overexpression of *lytABC* was done by amplification of *lytABC* with P647 and P648 and inserted between SalI and SphI restriction sites. Constructions were transferred in *B. subtilis* 168 through natural competency, verified by PCR, and then transferred in NCIB3610.

Markerless deletion. Markerless deletion of *conG* was done using pminiMAD2 (50). Upstream and downstream fragments were amplified with primers P668 and P669 and with primers P670 and P674, respectively. The two fragments were fused by long-fragment homology PCR and inserted into pminiMAD2 between the BamHI and EcoRI restriction sites. Plasmid pJSB19 was inserted into MM294, a *recA*$^+$ *E. coli*, to obtain concatemers. pJSB19 was then inserted into JMA384 by using natural competency and then incubated overnight with selection at 40°C. Multiple colonies were then incubated in LB broth for 3 to 4 h at room temperature and diluted into fresh LB broth overnight at room temperature. Excision and curing of the plasmid were achieved by successive passages and growth at 37°C. Cells were then plated on LB agar, and colonies were streaked on LB with and without MLS. Colonies that lost antibiotic resistance were then PCR verified to confirm the deletion of *conG*. Sequencing of the deleted locus was also performed.

Biofilm matings. Donor and recipient cells were grown from a single colony in 3 mL LB broth at 37°C to late exponential phase (3 to 4 h), diluted at an OD$_{600}$ of 1.5 in 1$\times$ PBS (137 mM NaCl, 2.7 mM KCl, 10 mM Na_2HPO_4, and 1.8 mM KH_2PO_4, pH 7.4) and mixed at a 1:5 donor-to-recipient ratio unless indicated otherwise. Cells were then centrifuged for 3 min at 5,000 rpm, and the pellet was resuspended in 1/10th of the volume. Ten microliters of the mix was dropped onto the appropriate medium and incubated for 20 h (unless time specified [Fig. 2 and 3]) at 30°C. When necessary, expression of the different constructs was induced by adding IPTG (isopropyl β-D-1-thiogalactopyranoside) to the medium. Fluorescent constructions were induced by adding 50 μM IPTG to both the liquid preculture and biofilm

medium (Fig. 1, 3, and 4; Fig. S2; Video S1). Complementation of *conG* was done by adding 50 μM IPTG to the biofilm-inducing medium (Fig. 5).

To determine conjugation levels, colonies were collected from agar media with a bent pipette tip and put in 1 mL 1× PBS and then sonicated at 30% amplitude for 20 s twice with a 1:1 pulse. Cell suspensions were serially diluted and plated on LB with the appropriate antibiotic and allowed to grow until the next day. Donor, recipient, and transconjugant CFU were then counted. The frequency of transconjugants formation was expressed as a function of the number of recipients CFU (number of transconjugants divided by the number of recipient CFU) because transconjugants are an important actor in the propagation of ICE*Bs1* (Fig. 4).

Thin section. Preparation of the mating assay was done as previously described, but 2 μL instead of 10 μL of the mixture was dropped on MSgg medium with 1.5% (wt/vol) agar poured into 6-well plates. At the appropriate time, biofilms were fixed using paraformaldehyde 4% (wt/vol) for 10 min and washed twice with PBS. Samples of biofilm and agar were harvested from the plates and transferred into a homemade aluminum foil mold, overlaid with Tissue-Plus optimal cutting temperature (OCT) compound clear (catalog no. 4585; Thermo Fisher), and fast-frozen on dry ice. The frozen samples were stored at −80°C before being sent to Plateforme d'histologie de l'Université de Sherbrooke and sliced into 8-μm-thick slices using a cryomicrotome set to −20°C. Thin sections were placed on a positively charged slide (Globe Scientific Inc.; catalog no. no. 1358W), and an aqueous mounting medium was added (0.5% [wt/vol] *N*-propyl gallate, 50% [vol/vol] glycerol, and PBS) and covered with a number 1.5 coverslip. Slides were kept at 4°C prior to imaging. Thin sections were analyzed using an Olympus FV3000 confocal microscope at ×60 magnification using PlanApo objective (60×, 1.4 numerical aperture [NA]) with the following laser settings: 405 nm, 488 nm, and 561 nm. Laser intensity and sensor sensitivity were the same under all conditions. Fields of view are composed of multiple pictures taken sequentially to cover the area of the biofilm. To allow stitching of the picture together and form a large field of view, the overlapping region between 2 pictures needs to be imaged twice causing small bleaching of the area in the second picture. As the software used for the stitching calculated the mean of the overlapping region, some darker lines appeared at the border of two individual pictures (Fig. 3A). The distances separating the conjugative clusters with either the air-biofilm or biofilm-media interface were measured using the ImageJ software. The relative distance was calculated as the distance measure divided by the total thickness of the biofilm at the area of the picture taken.

Inverted microscopy on biofilm. Preparation of the mating assay was done as previously described, but 2 μL instead of 10 μL of the mixture was dropped on MSgg or MSNc medium with 1.5% (wt/vol) agar. At the appropriate time point, agar containing the biofilm was cut with a razor blade. Excess agar was removed carefully before inversion of the whole biofilm into a 35-mm petri dish containing a coverglass number 1.5 (part no. P35G-1.5-14C; MatTek Corporation). Pictures of the inner part of the biofilms were taken using an Olympus FV3000 confocal microscope at ×60 magnification (PlanApo objective [60×, 1.4 NA]) with the following laser settings: 405 nm, 488 nm, and 561 nm. Laser intensity and sensor sensitivity were the same for all conditions. For statistical analysis, bacteria were counted using ImageJ software with a cell counter plugin.

Statistical analysis. Statistical analyses were performed using GraphPad Prism 9. Comparisons were done as specified in the figure legends.

SUPPLEMENTAL MATERIAL

Supplemental material is available online only.
SUPPLEMENTAL FILE 1, PDF file, 4.3 MB.
SUPPLEMENTAL FILE 2, AVI file, 0.2 MB.

ACKNOWLEDGMENTS

REFERENCES

1. Ochman H, Lawrence JG, Groisman EA. 2000. Lateral gene transfer and the nature of bacterial innovation. Nature 405:299–304. https://doi.org/10.1038/35012500.
2. Frost LS, Leplae R, Summers AO, Toussaint A. 2005. Mobile genetic elements: the agents of open source evolution. Nat Rev Microbiol 3:722–732. https://doi.org/10.1038/nrmicro1235.
3. Babic A, Berkmen MB, Lee CA, Grossman AD. 2011. Efficient gene transfer in bacterial cell chains. mBio 2:27–38. https://doi.org/10.1128/mBio.00027-11.
4. Hausner M, Wuertz S. 1999. High rates of conjugation in bacterial biofilms as determined by quantitative in situ analysis. Appl Environ Microbiol 65:3710–3713. https://doi.org/10.1128/AEM.65.8.3710-3713.1999.
5. Gaillard M, Vallaeys T, Vorhölter FJ, Minoia M, Werlen C, Sentchilo V, Pühler A, Van Meer Der JR. 2006. The clc element of Pseudomonas sp. strain B13, a genomic island with various catabolic properties. J Bacteriol 188:1999–2013. https://doi.org/10.1128/JB.188.5.1999-2013.2006.

6. Martínez JL, Baquero F. 2014. Emergence and spread of antibiotic resistance: setting a parameter space. Ups J Med Sci 119:68–77. https://doi.org/10.3109/03009734.2014.901444.

7. Liu D, Yang Y, Gu J, Tuo H, Li P, Xie X, Ma xu G, Liu J, Zhang A. 2019. The Yersinia high-pathogenicity island (HPI) carried by a new integrative and conjugative element (ICE) in a multidrug-resistant and hypervirulent Klebsiella pneumoniae strain SCsl1. Vet Microbiol 239:108481. https://doi.org/10.1016/j.vetmic.2019.108481.

8. Botelho J, Schulenburg H. 2021. The role of integrative and conjugative elements in antibiotic resistance evolution. Trends Microbiol 29:8–18. https://doi.org/10.1016/j.tim.2020.05.011.

9. Auchtung JM, Lee CA, Monson RE, Lehman AP, Grossman AD. 2005. Regulation of a Bacillus subtilis mobile genetic element by intercellular signaling and the global DNA damage response. Proc Natl Acad Sci U S A 102: 12554–12559. https://doi.org/10.1073/pnas.0505835102.

10. Burrus V, Pavlovic G, Decaris B, Guédon G. 2002. The ICESt1 element of Streptococcus thermophilus belongs to a large family of integrative and conjugative elements that exchange modules and change their specificity of integration. Plasmid 48:77–97. https://doi.org/10.1016/s0147-619x(02)00102-6.

11. Auchtung JM, Aleksanyan N, Bulku A, Berkmen MB. 2016. Biology of ICEBs1, an integrative and conjugative element in Bacillus subtilis. Plasmid 86:14–25. https://doi.org/10.1016/j.plasmid.2016.07.001.

12. Auchtung JM, Lee CA, Garrison KL, Grossman AD. 2007. Identification and characterization of the immunity repressor (ImmR) that controls the mobile genetic element ICEBs1 of Bacillus subtilis. Mol Microbiol 64: 1515–1528. https://doi.org/10.1111/j.1365-2958.2007.05748.x.

13. van Gestel J, Bareia T, Tenennbaum B, Dal Co A, Guler P, Aframian N, Puyesky S, Grinberg I, D'Souza GG, Erez Z, Ackermann M, Eldar A. 2021. Short-range quorum sensing controls horizontal gene transfer at micron scale in bacterial communities. Nat Commun 12:2324. https://doi.org/10.1038/s41467-021-22649-4.

14. Lee CA, Auchtung JM, Monson RE, Grossman AD. 2007. Identification and characterization of int (integrase), xis (excisionase) and chromosomal attachment sites of the integrative and conjugative element ICEBs1 of Bacillus subtilis. Mol Microbiol 66:1356–1369. https://doi.org/10.1111/j.1365-2958.2007.06000.x.

15. Lee CA, Grossman AD. 2007. Identification of the origin of transfer (oriT) and DNA relaxase required for conjugation of the integrative and conjugative element ICEBs1 of Bacillus subtilis. J Bacteriol 189:7254–7261. https://doi.org/10.1128/JB.00932-07.

16. Leonetti CT, Hamada MA, Laurer SJ, Broulidakis MP, Swerdlow KJ, Lee CA, Grossman AD, Berkmen MB. 2015. Critical components of the conjugation machinery of the integrative and conjugative element ICEBs1 of Bacillus subtilis. J Bacteriol 197:2558–2567. https://doi.org/10.1128/JB.00142-15.

17. Chandler M, De La Cruz F, Dyda F, Hickman AB, Moncalian G, Ton-Hoang B. 2013. Breaking and joining single-stranded DNA: the HUH endonuclease superfamily. Nat Rev Microbiol 11:525–538. https://doi.org/10.1038/nrmicro3067.

18. Draper O, César CE, Machón C, De La Cruz F, Llosa M. 2005. Site-specific recombinase and integrase activities of a conjugative relaxase in recipient cells. Proc Natl Acad Sci U S A 102:16385–16390. https://doi.org/10.1073/pnas.0506081102.

19. Wright LD, Johnson CM, Grossman AD. 2015. Identification of a single strand origin of replication in the integrative and conjugative element ICEBs1 of Bacillus subtilis. PLoS Genet 11:e1005556. https://doi.org/10.1371/journal.pgen.1005556.

20. Avello M, Davis KP, Grossman AD. 2019. Identification, characterization and benefits of an exclusion system in an integrative and conjugative element of Bacillus subtilis. Mol Microbiol 112:1066–1082. https://doi.org/10.1111/mmi.14359.

21. Hall-Stoodley L, Costerton JW, Stoodley P. 2004. Bacterial biofilms: from the natural environment to infectious diseases. Nat Rev Microbiol 2: 95–108. https://doi.org/10.1038/nrmicro821.

22. Stewart PS, Franklin MJ. 2008. Physiological heterogeneity in biofilms. Nat Rev Microbiol 6:199–210. https://doi.org/10.1038/nrmicro1838.

23. Høiby N, Bjarnsholt T, Givskov M, Molin S, Ciofu O. 2010. Antibiotic resistance of bacterial biofilms. Int J Antimicrob Agents 35:322–332. https://doi.org/10.1016/j.ijantimicag.2009.12.011.

24. Vlamakis H, Aguilar C, Losick R, Kolter R. 2008. Control of cell fate by the formation of an architecturally complex bacterial community. Genes Dev 22:945–953. https://doi.org/10.1101/gad.1645008.

25. Nocelli N, Bogino PC, Banchio E, Giordano W. 2016. Roles of extracellular polysaccharides and biofilm formation in heavy metal resistance of rhizobia. Materials (Basel) 9:418. https://doi.org/10.3390/ma9060418.

26. Molin S, Tolker-Nielsen T. 2003. Gene transfer occurs with enhanced efficiency in biofilms and induces enhanced stabilisation of the biofilm structure. Curr Opin Biotechnol 14:255–261. https://doi.org/10.1016/s0958-1669(03)00036-3.

27. Virolle C, Goldlust K, Djermoun S, Bigot S, Lesterlin C. 2020. Plasmid transfer by conjugation in Gram-negative bacteria: from the cellular to the community level. Genes (Basel) 11:1239. https://doi.org/10.3390/genes11111239.

28. Li B, Qiu Y, Zhang J, Huang X, Shi H, Yin H. 2018. Real-time study of rapid spread of antibiotic resistance plasmid in biofilm using microfluidics. Environ Sci Technol 52:11132–11141. https://doi.org/10.1021/acs.est.8b03281.

29. Christensen BB, Sternberg C, Andersen JB, Eberl L, Møller S, Givskov M, Molin S. 1998. Establishment of new genetic traits in a microbial biofilm community. Appl Environ Microbiol 64:2247–2255. https://doi.org/10.1128/AEM.64.6.2247-2255.1998.

30. Zhu L, Chen T, Xu L, Zhou Z, Feng W, Liu Y, Chen H. 2020. Effect and mechanism of quorum sensing on horizontal transfer of multidrug plasmid RP4 in BAC biofilm. Sci Total Environ 698:134236. https://doi.org/10.1016/j.scitotenv.2019.134236.

31. Stalder T, Top E. 2016. Plasmid transfer in biofilms: a perspective on limitations and opportunities. NPJ Biofilms Microbiomes 2:16022. https://doi.org/10.1038/npjbiofilms.2016.22.

32. Qiu Y, Zhang J, Li B, Wen X, Liang P, Huang X. 2018. A novel microfluidic system enables visualization and analysis of antibiotic resistance gene transfer to activated sludge bacteria in biofilm. Sci Total Environ 642: 582–590. https://doi.org/10.1016/j.scitotenv.2018.06.012.

33. Lécuyer F, Bourassa J-S, Gélinas M, Charron-Lamoureux V, Burrus V, Beauregard PB. 2018. Biofilm formation drives transfer of the conjugative element ICEBs1 in Bacillus subtilis. mSphere 3:e00473-18. https://doi.org/10.1128/mSphere.00473-18.

34. Kearns DB, Chu F, Branda SS, Kolter R, Losick R. 2005. A master regulator for biofilm formation by Bacillus subtilis. Mol Microbiol 55:739–749. https://doi.org/10.1111/j.1365-2958.2004.04440.x.

35. Jones JM, Grinberg I, Eldar A, Grossman AD. 2021. A mobile genetic element increases bacterial host fitness by manipulating development. Elife 10:1–24. https://doi.org/10.7554/eLife.65924.

36. Huguet KT, Rivard N, Garneau D, Palanee J, Burrus V. 2020. Replication of the Salmonella genomic island 1 (SGI1) triggered by helper IncC conjugative plasmids promotes incompatibility and plasmid loss. PLoS Genet 16: e1008965. https://doi.org/10.1371/journal.pgen.1008965.

37. Hernandez-Beltran JCR, Rodríguez-Beltrán J, Millán AS, Peña-Miller R, Fuentes-Hernández A. 2021. Quantifying plasmid dynamics using single-cell microfluidics and image bioinformatics. Plasmid 113:102517. https://doi.org/10.1016/j.plasmid.2020.102517.

38. Branda SS, González-Pastor JE, Ben-Yehuda S, Losick R, Kolter R. 2001. Fruiting body formation by Bacillus subtilis. Proc Natl Acad Sci U S A 98: 11621–11626. https://doi.org/10.1073/pnas.191384198.

39. Yamamoto H, Kurosawa SI, Sekiguchi J. 2003. Localization of the vegetative cell wall hydrolases LytC, LytE, and LytF on the Bacillus subtilis cell surface and stability of these enzymes to cell wall-bound or extracellular proteases. J Bacteriol 185:6666–6677. https://doi.org/10.1128/JB.185.22.6666-6677.2003.

40. Vollmer W, Joris B, Charlier P, Foster S. 2008. Bacterial peptidoglycan (murein) hydrolases. FEMS Microbiol Rev 32:259–286. https://doi.org/10.1111/j.1574-6976.2007.00099.x.

41. Bose B, Auchtung JM, Lee CA, Grossman AD. 2008. A conserved antirepressor controls horizontal gene transfer by proteolysis. Mol Microbiol 70:570–582. https://doi.org/10.1111/j.1365-2958.2008.06414.x.

42. Reinhard F, Miyazaki R, Pradervand N, Van Der Meer JR. 2013. Cell differentiation to "mating bodies" induced by an integrating and conjugative element in free-living bacteria. Curr Biol 23:255–259. https://doi.org/10.1016/j.cub.2012.12.025.

43. François D, Roxane M, van der Roelof MJ, BM J. 2021. Transient replication in specialized cells favors transfer of an integrative and conjugative element. mBio 10:e01133-19. https://doi.org/10.1128/mBio.01133-19.

44. Lee CA, Babic A, Grossman AD. 2010. Autonomous plasmid-like replication of a conjugative transposon. Mol Microbiol 75:268–279. https://doi.org/10.1111/j.1365-2958.2009.06985.x.

45. Rivard N, Colwell RR, Burrus V. 2020. Antibiotic resistance in Vibrio cholerae: mechanistic insights from IncC plasmid-mediated dissemination of a novel family of genomic islands inserted at trmE. mSphere 5:e1008965. https://doi.org/10.1128/mSphere.00748-20.

46. Humbert M, Huguet KT, Coulombe F, Burrus V. 2019. Entry exclusion of conjugative plasmids of the IncA, IncC, and related untyped incompatibility groups. J Bacteriol 209:e00731-18. https://doi.org/10.1128/JB.00731-18.

47. Kohler V, Probst I, Aufschnaiter A, Büttner S, Schaden L, Rechberger GN, Koraimann G, Grohmann E, Keller W. 2017. Conjugative type IV secretion

in Gram-positive pathogens: traG, a lytic transglycosylase and endopepti-dase, interacts with translocation channel protein TraM. Plasmid 91:9–18. https://doi.org/10.1016/j.plasmid.2017.02.002.

48. Beauregard PB, Chai Y, Vlamakis H, Losick R, Kolter R. 2013. Bacillus subtilis biofilm induction by plant polysaccharides. Proc Natl Acad Sci U S A 110:E1621–E1630. https://doi.org/10.1073/pnas.1218984110.

49. Yasbin RE, Young FE. 1974. Transduction in Bacillus subtilis by bacteriophage SPP1. J Virol 14:1343–1348. https://doi.org/10.1128/JVI.14.6.1343-1348.1974.

50. Patrick JE, Kearns DB. 2008. MinJ (YvjD) is a topological determinant of cell division in Bacillus subtilis. Mol Microbiol 70:1166–1179. https://doi.org/10.1111/j.1365-2958.2008.06469.x.